Journal of the Optical Society of America B
OPTICAL PHYSICS

Temporal reflection from short pump pulses inside a dispersive nonlinear medium: the impact of pump parameters

JUNCHI ZHANG,[1,*] WILLIAM R. DONALDSON,[2] AND GOVIND P. AGRAWAL[1]

[1]The Institute of Optics, University of Rochester, Rochester, New York 14627, USA
[2]Laboratory for Laser Energetics, University of Rochester, Rochester, New York 14627, USA
*jzh156@ur.rochester.edu

Received 19 April 2024; revised 26 June 2024; accepted 13 July 2024; posted 15 July 2024; published 29 July 2024

We have studied, through a series of experiments and numerical simulations, how temporal reflection from an intense pump pulse inside a photonic crystal fiber is affected by parameters of the pump pulse used to form a moving high-index boundary. We used femtosecond pump pulses, which slow down inside the fiber as their spectrum red-shifts because of intrapulse Raman scattering. Temporal reflection of probe pulses occurs from such decelerating pump pulses. We changed the width and chirp of our pump pulses with a 4f pulse shaper capable of providing both spectral filtering and frequency chirping. We found that temporal refection exhibited novel features, to our knowledge, when pump pulses were made wider or chirped. In both cases, two or more reflected pulses were produced at different wavelengths in a specific range of the initial pump-probe delays. Numerical simulations reveal that the origin of such novel features is related to the complex nonlinear evolution of pump pulses inside optical fibers.

https://doi.org/10.1364/JOSAB.528062

1. INTRODUCTION

Considerable attention has been paid recently to wave propagation in a time-varying medium [1–7]. In most studies, the refractive index of the whole medium is assumed to be modulated on the single-cycle time scale, resulting in temporal reflection and refraction with some frequency shift from the incident wave [8–10]. By changing the medium's refractive index in a periodic fashion, it is even possible to form a photonic time crystal [11–13]. Although such temporal reflection has been observed at low frequencies using water waves [14], microwaves [15], or ultra cold atoms [16], it is hard to observe this phenomenon at high frequencies lying in the optical region.

This issue can be resolved through traveling-wave modulation, which changes the medium's refractive index, both in space and time, at the speed of the traveling wave [17–19]. The simplest situation corresponds to a moving index boundary with different refractive indices on its two sides. When an optical pulse interacts with this type of boundary inside a dispersive medium, it splits into two parts, whose frequencies are shifted such that they travel at different speeds [20–23]. These two parts correspond to transmitted and reflected pulses and are temporal analogs of the reflection and refraction at a spatial boundary [17]. This type of temporal reflection does not require index modulation to occur on a single-cycle time scale, and it is also possible to realize total internal reflection. In this paper, we consider only the second type of temporal reflection occurring at a moving refractive index boundary.

Temporal reflection from a moving index boundary has been observed using the nonlinear effects and identified as the optical analog of an event horizon [24–27]. In this case, a strong pump pulse is sent into a dispersive nonlinear medium, such as an optical fiber, and a change in the local refractive index is created through the optical Kerr effect. Each pump pulse increases the medium's refractive index in a time window set by its width, and this window moves at the speed of the pump pulse. When a probe pulse, moving at different speed because of its different wavelength, interacts with this index window, a reflected pulse is generated at a shifted wavelength from that of the probe. In a recent study [28], we used such wavelength shifts to deduce the trajectory of a Raman soliton by sending an intense pump pulse into a photonic crystal fiber (PCF) such that it formed a soliton whose speed decreased with propagation because of intrapulse Raman scattering [29].

Even though temporal reflection from a moving index boundary is well understood by now [17,22], the situation is different when a pump pulse is used to create a time window whose shape and duration depend on the pump pulse itself. Although one would expect the properties of a reflected pulse to depend on the parameters of a pump pulse (such as its width and chirp), this issue has not yet attracted much attention. In this work, we carry out a detailed experimental and numerical

study to understand how the width and chirp of a pump pulse influence the temporal reflection process. Our results show that both of these pump parameters affect significantly temporal reflection of a probe pulse because of different evolution dynamics of the pump pulse propagation inside the PCF used for our experiments. As an example, multiple reflected pulses may be generated at different wavelengths in some specific cases. Our numerical simulations agree well with our experiments in all cases we studied. The paper is organized as follows. Section 2 describes the physics behind temporal reflection together with a pump-probe model that can be used to study this phenomenon numerically. Section 3 provides details of our experimental setup and discusses the ideal case of temporal reflection from a pump pulse propagating as a fundamental soliton inside the PCF. In Section 4, we discuss how temporal reflection is affected when pump pulses are made wider through spectral filtering or chirped using a dispersive delay line. The main conclusions are summarized in Section 5.

2. PHYSICS AND MODELING OF TEMPORAL REFLECTION

The simplest way to understand the phenomenon of temporal reflection is to consider a sharp moving boundary inside a dispersive medium with different refractive indices on its two sides, as shown in Fig. 1(a) schematically. An optical pulse, traveling faster than this boundary, interacts with it and is split into two parts, one of which corresponds to a reflected pulse that never crosses the index boundary. Unlike the Doppler effect associated with a moving medium, the reflected pulse still travels in the forward direction, but it travels slower than the index boundary. This effect is possible only in a dispersive medium and occurs because of a change in the wavelength of the reflected pulse. Some energy of the incoming pulse appears on the other side of the boundary as a transmitted pulse, as shown in Fig. 1(a). Under some conditions, the transmitted part can be completely suppressed, resulting in the temporal analog of the total internal reflection [17].

The central frequency of both the reflected and transmitted pulses shifts from that of the incident pulse because a moving boundary breaks the time-translation symmetry. The frequencies of these pulses can be found by considering the phase continuity relation [2]. In essence, during the reflection process, the phase difference between the incident, reflected, and transmitted waves should remain the same along the trajectory of the boundary. This requirement leads to the following relation:

$$\frac{\omega_r - \omega_i}{\beta_r - \beta_i} = \frac{\omega_t - \omega_i}{\beta_t - \beta_i} = v_b, \tag{1}$$

where v_b stands for the speed of the index boundary and ω_k and β_k represent the frequency and the propagation constant of the three waves for $k = i, r, t$. This relation is shown graphically in Fig. 1(b), where the two curves represent the dispersion relations of the medium on two sides of the boundary. The arrow points to the frequency ω_i of the incoming wave. To find the frequencies of the reflected and transmitted waves, we use Eq. (1) to draw a dashed line with the slope v_b, and intersection of this line with the two curves provides the corresponding frequencies. In the example shown, no transmitted wave forms because the dashed line does not intersect with the bottom curve. This situation corresponds to 100% reflection of the incident pulse and produces a reflected pulse at the shifted frequency ω_r such that it moves slower than the boundary. It is worth noting that such temporal reflection can only occur in a dispersive medium. It is apparent from Eq. (1) that the frequency shifts of the reflected and transmitted pulses depend on the speed v_b of the boundary. A larger mismatch between speeds of the incident pulse and the boundary may lead to a larger frequency shift of the reflected wave but this usually leads to a smaller reflectivity. In general, a trade-off exists between the efficiency of the temporal reflection and the magnitude of frequency shift.

To simulate the temporal reflection process inside an optical fiber, we use the generalized nonlinear Schrödinger equation, which includes all higher-order effects such as cubic dispersion and intrapulse Raman scattering [29]. As the pump and probe pulses used in our experiment have wavelengths far apart that their spectra do not overlap, we can write the total electric field in the form

$$E(z, t_a) = \mathrm{Re}\left(A_s(z, t_a)e^{i[\beta(\omega_s)z - \omega_s t_a]} + A_p(z, t_a)e^{i[\beta(\omega_p)z - \omega_p t_a]}\right), \tag{2}$$

where t_a is the time in the laboratory frame, ω_s and ω_p are the reference frequencies of the pump (soliton) and probe pulses for the definition of envelopes, and A_s and A_p are the corresponding envelopes. The reference frequencies do not need to be the same as the central frequencies of the pulses. They only need to lie near the pulse spectrum. Assuming that the probe's energy is small enough that its nonlinear effects can be neglected, the following set of two coupled nonlinear equations describes the propagation of two pulses quite accurately:

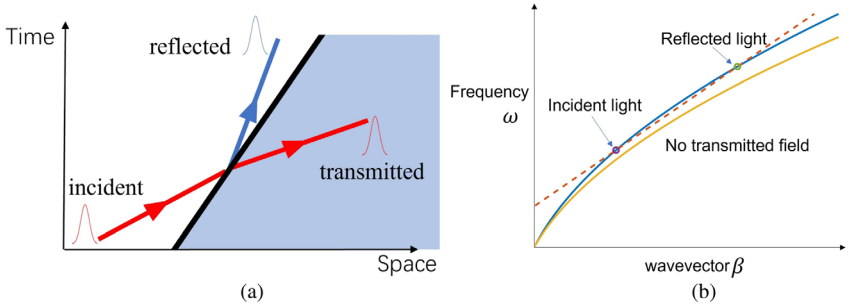

Fig. 1. (a) Schematic showing temporal reflection (blue line) of an incoming optical pulse (red line) from a moving boundary (thick black line) in a dispersive medium. (b) Phase-continuity relation (dashed line) in the $\beta - \omega$ space. The blue and yellow lines show the dispersion curves on the opposite sides of the moving boundary when the condition for total internal reflection is satisfied. This figure is taken from Ref. [28].

$$\frac{\partial A_s}{\partial z}+\sum_{k\geq 2}\frac{i^{k-1}}{k!}\beta_k^{(s)}\frac{\partial^k A_s}{\partial t^k}=i\gamma[(1-f_R)|A_s|^2A_s+f_R N_R A_s], \tag{3}$$

$$\frac{\partial A_p}{\partial z}+\Delta\beta_1\frac{\partial A_p}{\partial t}+\sum_{k\geq 2}\frac{i^{k-1}}{k!}\beta_k^{(p)}\frac{\partial^k A_p}{\partial t^k}=2i\gamma|A_s|^2A_p, \tag{4}$$

where $t=t_a-z/v_s$ is the reduced time in a frame moving with the group velocity v_s of the pump pulse and γ is the nonlinear parameter. Dispersive effects are included through multiple parameters defined as $\beta_k^{(j)}=(d^k\beta/d\omega^k)|_{\omega_j}$ $(j=s,p)$ at the pump and probe's reference frequencies. The parameter $\Delta\beta_1=(d\beta/d\omega)|_{\omega_p}-(d\beta/d\omega)|_{\omega_s}$ is related to the difference of the pump and probe's group velocity between the two reference frequencies.

The effects of intrapulse Raman scattering are included in Eq. (3) through the Raman term $N_R=\int_0^\infty h_R(t')|A_s(z,t-t')|^2dt'$, where $h_R(t)$ is the Raman response function. The parameter f_R sets the relative weight of the Raman contribution. We used the functional form of $h_R(t)$ with the f_R value given in Ref. [29]. We did not include the effects of self steepening in our simulations because we found them negligible in all cases we studied. The probe pulse is affected by the pump through the cross-phase modulation term in Eq. (4).

It is worth discussing the validity of the assumption that evolution of a pump pulse is unaffected by the probe pulse. Experimentally, we kept energy of probe pulses relatively low. We also compared the spectra of pump pulses recorded with and without launching probe pulses and ensured that no observable changes were induced by probe pulses. We can deduce a simple rule of thumb that we can use to check if we would expect the effect of a probe pulse on the pump pulse to be non-negligible. The probe can affect the pump pulse through cross-phase modulation, and it is a time derivative of the phase that is important for the pump pulse's evolution. Thus, we can compare the ratio P/T for the pump and probe pulses, where P is the pulse's peak power and T is its temporal width. Equivalently, we can compare the ratio E/T^2 for the two pulses, where E stands for pulse's energy. For our experiment, this ratio was smaller for the probe pulse by a factor of 50. This justifies the assumption made in Eq. (3).

3. EXPERIMENTS AND SIMULATIONS

We used a 3.8-m-long PCF (IXblue, IXF-SUP-2-135) for observing temporal reflection. Since its dispersive properties are of paramount importance, we characterized this PCF by measuring its group delay over a wide frequency range with the technique of white-light interferometry [30,31]. The results are shown in Fig. 2. The slope of this curve at any frequency provides the value of β_2 at that frequency. This slope or β_2 vanishes at the zero-dispersion frequency (406 THz, or 739 nm) where group delay is minimum. This frequency separates the anomalous- and normal-dispersion regions depending on whether β_2 is negative or positive.

To create a moving time window with a larger refractive index through the optical Kerr effect, we launch an intense short pump pulse in the anomalous-dispersion region of the PCF.

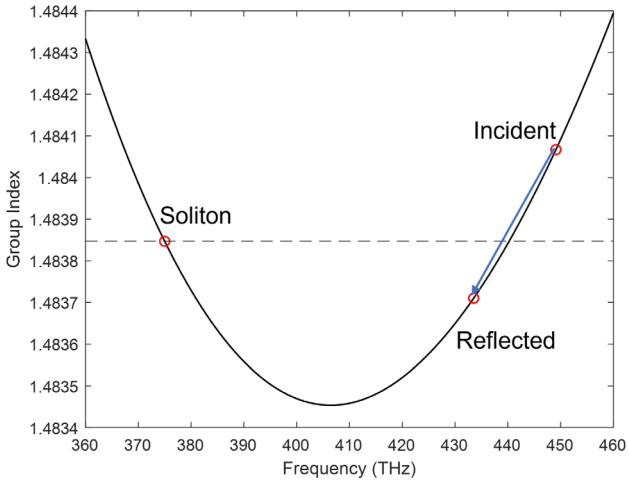

Fig. 2. Measured group index of the PCF plotted as a function of frequency. Its values at the frequencies of the pump, probe, and reflected pulses are marked by three circles.

We also launch a much weaker probe pulse into the PCF at a different wavelength. We chose 800 nm as the wavelength of pump pulses because it lies in the anomalous region and allows the formation of an optical soliton inside our PCF. The probe's wavelength was chosen in the normal-dispersion region such that both pulses traveled with a small speed difference. In all cases throughout this paper, we used probe pulses weak enough that it has negligible impact on the propagation of the pump pulse. As seen in Fig. 2, a probe pulse traveling slower than the soliton produces a reflected pulse moving faster than the soliton after its encounter with the soliton. By contrast, a probe pulse traveling faster than the soliton produces a reflected pulse moving slower than the soliton.

Figure 3(a) shows our experimental setup. A Ti:sapphire laser regenerative amplifier (Coherent, Astrella) is used as a source of femtosecond pulses. It generates 30–40-fs pulses of about 7 mJ of energy at a wavelength of 800 nm. A very small portion of the energy is split off and used for the pump pulse. A half of the energy is sent into an optical parametric amplifier (OPA) that can generate pulses with tunable wavelength from 200 to 2000 nm. The probe pulses used in our experiment are from this OPA. We set the OPA to work in the range of 600–700 nm and placed a bandpass filter at the output of the OPA to limit the spectral bandwidth to about 5 nm.

Pump pulses from the Ti:sapphire laser are sent into a pulse-shaping setup shown in Fig. 3(b). This pulse is used as the pump pulse for our experiment. It is a double-pass 4f system containing two prisms, two lenses, and a mirror. One prism separates spatially different spectral components of the pulse, and the second prism brings them together after spectral filtering through a tunable slit. A geometrical path difference of different spectral components introduces some dispersion into the system, which can be controlled by translating one of the prisms [32]. A linear polarizer is placed in front of the PCF to ensure that the polarization states of the pump and probe pulses are aligned with the slow axis of the PCF. The group delay offset caused by the linear polarizer is taken into account by calculating this offset based on the material and thickness. To ensure that the two pulses have a fixed relative delay, a translation stage

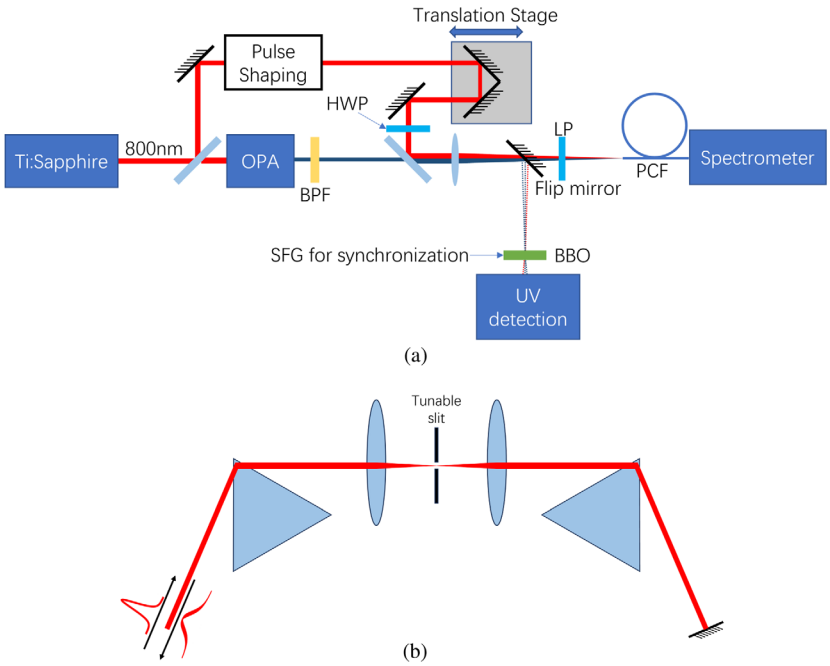

Fig. 3. Experimental setup. (a) Schematic of the experimental setup. OPA: optical parametric amplifier; BPF: band-pass filter; HWP: half-wave plate; LP: linear polarizer; SHG: sum-frequency generation; BBO: barium borate. (b) Details of the pulse shaping part in (a). It is a double-pass 4f system containing two prisms, two lenses, and a mirror. A tunable slit is placed at the Fourier plane of the 4f system for spectral manipulation. One of the prisms is mounted on a translational stage for dispersion control.

was used. We also used a BBO crystal for sum frequency generation and temporal synchronization. The zero-delay position corresponded to the maximum of the generated signal.

In this section, we focus on the ideal case where each pump pulse forms a fundamental soliton, whose spectrum shifts toward the red side with propagation inside the PCF because of intrapulse Raman scattering. Numerical simulations are based on the pump-probe coupled equations given in Section 2. The pump pulse at the front end of the fiber has the form of a fundamental soliton:

$$A_1(0,t) = \sqrt{P_1}\,\mathrm{sech}(t/T_1), \qquad P_1 = |\beta_2^{(s)}|/(\gamma T_1^2). \tag{5}$$

We used $T_1 = 17.3$ fs to match the 30-fs width of our pump pulses with an initial delay of 0.33 ps. The nonlinear coefficient $\gamma = 105\ \mathrm{W^{-1}km^{-1}}$. The probe pulse was in the form of a Gaussian pulse with a 5-nm-wide spectrum centered at the 655-nm wavelength. Its energy was low enough that it did not affect the pump pulse. The probe's energy was kept small and was only about 6% of that of the pump pulse in our experiments.

Figure 4 shows the numerical results by plotting the temporal and spectral evolution over the PCF length for the pump (top) and probe (bottom) pulses. The pump pulse maintains its width because it forms a soliton whose spectrum shifts continuously toward the red side as it propagates down the fiber. This red shift, together with the anomalous dispersion, slows down the pump pulse, resulting in a trajectory bent toward the right side. At the output end of the fiber, the soliton's spectrum has shifted by more than 30 THz, and the 30-fs pump pulse has been delayed by 6 ps. The interesting question is how such a decelerating soliton affects the probe pulse, which would simply broaden in the absence of the pump pulse, with no changes occurring in its spectrum.

The bottom row in Fig. 4 shows clearly that the probe is affected considerably by the pump pulse. Nothing happens to the probe pulse, until the pump pulse traveling faster than the probe collides with it near $z = 25$ cm, and a reflected pulse is generated. This reflected pulse travels faster than the pump pulse because its spectrum has been shifted by more than 20-THz shift from that of the probe, as predicted by Eq. (1). The wide spectral peak, appearing after 0.25 m and located near 435 THz, corresponds to the reflected pulse. In the time domain, the reflected pulse spreads with further propagation (the blue band tilted toward the left) because its spectrum lies in the normal-dispersion region. This pulse never meets the pump pulse because it travels much faster than the pump.

However, that is not the case for the probe pulse, which collides with the pump pulse a second time at a distance of about 3 m. Interestingly, this collision produces a blue-shifted reflected pulse. This surprising behavior can be understood once we take into account Raman-induced deceleration of the pump pulse. During the first collision, the pump pulse is traveling faster than the probe. In contrast, the pump has slowed down so much at a distance of 3 m that its speed becomes lower than that of the probe. The collision forces the reflected pulse to travel slower than the pump, which is accompanied by the blue shift. Such multiple reflections leads to the trapping of the probe pulse by the pump pulse [33,34]. In this following discussion, we focus on the red-shifted portion of the probe pulse, occurring during its first collision with the pump pulse.

It should be clear by now that the spectral shift introduced during temporal reflection depends on the location within the

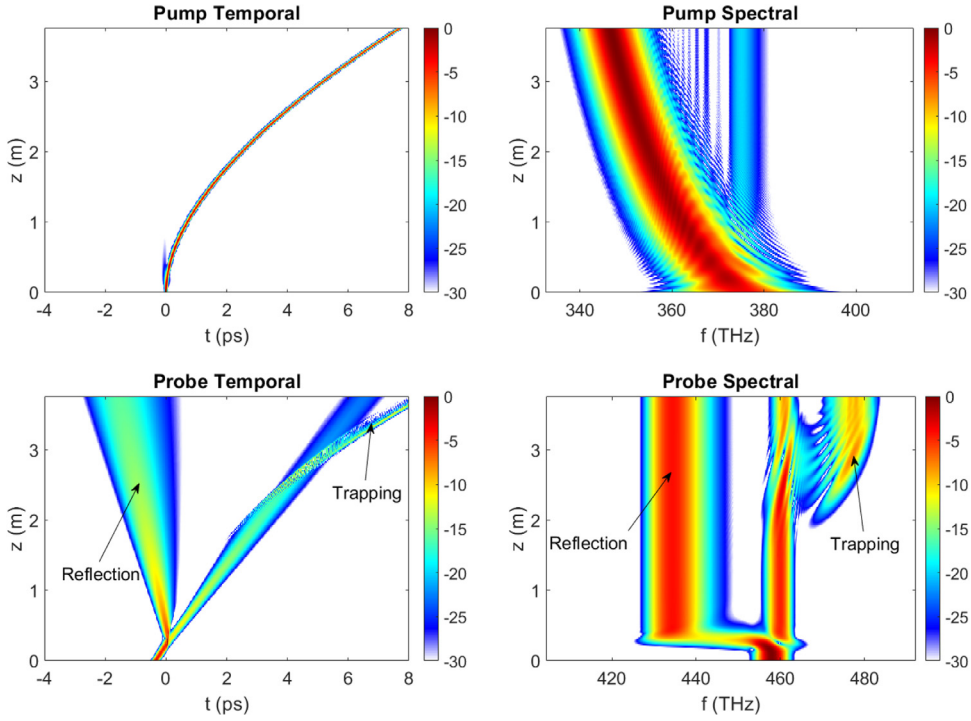

Fig. 4. Numerical simulations showing the temporal (left) and spectral (right) evolution of the pump (top) and probe (bottom) pulses over the PCF length. Pump pulse is launched at 800 nm and the probe's wavelength is 655 nm. Two pulses are delayed initially by 0.33 ps.

PCF where the pump and probe pulses collide. This location can be controlled by changing the probe's wavelength as well as the initial relative delay between the two pulses. Here, we keep the probe's wavelength fixed but change the relative delay over a 1-ps range. The probe's spectra, obtained numerically at the PCF's output end for different pump-probe delays, are shown in Fig. 5 as a color plot in which spectral intensity is color-coded on 20-dB scale. Three main spectral bands can be seen in this figure. The central band located near 650 nm corresponds to the probe pulse that is launched into the PCF together with the pump pulse (whose spectrum is not shown for clarity). The large spectral band on the right corresponds to the reflected pulse, generated during the first collision of the pump and probe. The spectral band on the left is marked trapping because it corresponds to a probe trapped by the pump pulse through multiple reflections. Note that the reflected pulse's spectral red shift becomes smaller for larger relative delays. This is because the pump pulse is decelerating as it propagates down the fiber. A larger delay forces the collision to occur at longer distances, where the pump slows down so much that its speed mismatch from the probe is decreased, resulting in a smaller frequency shift. We have shown earlier that the delay dependence of the reflected pulse spectrum can be used to deduce the decelerating trajectory of the soliton [28].

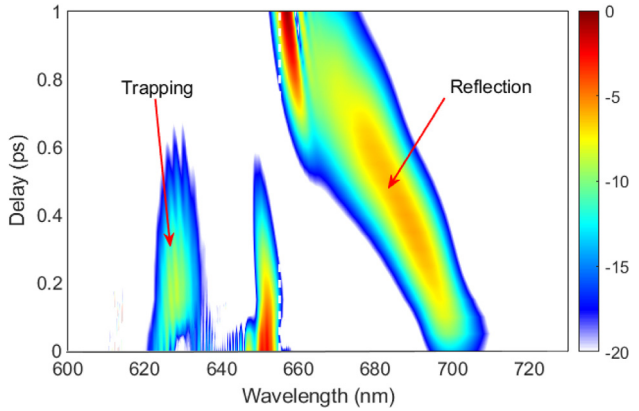

Fig. 5. Numerical simulations showing how output probe spectrum changes with the initial pump-probe delay. Positive delay implies that the pump is trailing the probe. White dashed line is the central wavelength of the input probe pulse.

Experimentally, we launched the pump and probe pulses using the setup shown in Fig. 3 and ensured that the pump pulse was intense enough to form a fundamental soliton. To achieve this, the slit in the pulse shaper was made wide enough that the pump's spectrum was not filtered. A prism in the pulse shaper was adjusted to compensate for the material's dispersion. We varied the initial delay of the pump pulse from the probe using the translation stage in Fig. 3 and recorded the spectra at the PCF's output end with a spectrometer.

Figure 6(a) shows the probe's spectra as the pump-probe delay changes and Fig. 6(b) shows the input and output spectra of the pump pulse for a specific delay. In Fig. 6(a), we experimentally varied the delay by an increment of 0.02 ps, and the data is plotted using the MATLAB function "pcolor". In Fig. 6(b), The input pump spectrum is centered at 800 nm but most of its energy appears at the output end of the PCF in a red-shifted peak centered near 865 nm. The 65-nm red shift of this Raman soliton agrees with numerical simulations shown in Fig. 4. We adjusted the pulse shaper to minimize the amount of energy left in the original 800-nm region, which depends on

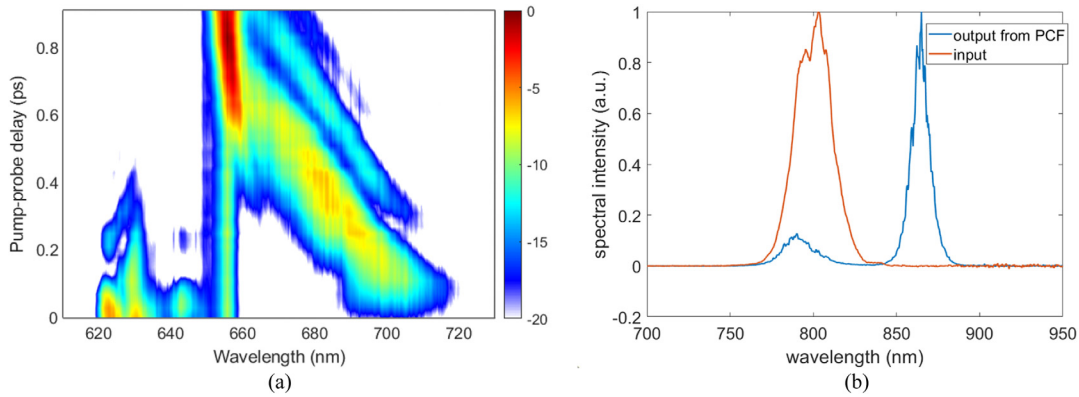

Fig. 6. (a) Experimental spectra of the probe pulse at the PCF output obtained for different pump-probe delays. (b) Spectra of the pump pulse at the input and output ends of the PCF.

the mismatch between the input pulse and the fundamental soliton. In our experiments, the energy of the pump pulse coupled into the PCF is estimated to be about 14.3 pJ, and 82% of this energy is converted into a Raman soliton that evolves as a fundamental soliton, (about 12 pJ at the output). In our simulation, we found that an output Raman soliton that has the same amount of Raman frequency shift would have an energy of about 14 pJ, in reasonable agreement with the experimental value. In simulations, we found that it is more suitable to adjust the input pulse energy so that the output Raman soliton has the same wavelength as in the experiment, since the Raman shift is a more direct indication of the strength of the nonlinearity that happened to the pulse.

The spectra in Fig. 6(a) were obtained for a probe pulse whose spectrum was centered at 655 nm with 5-nm bandwidth. This figure should be compared with numerical simulations shown in Fig. 5. Even though the two figures look different, the qualitative agreement is quite good. In both cases, a wide band on the right corresponds to the reflected pulse, the amount of red shift decreases as delay increases, and eventually the shift becomes so small that the spectrum of the reflected pulse merges with that of the probe. Further changes in the reflected pulse's spectrum occur in a continuous fashion as the delay is varied. This is consistent with simulations shown in Fig. 5 and occurs because the pump pulse, propagating as a fundamental soliton, creates a smooth boundary of index change for the probe pulse to reflect on.

We briefly comment on the items for which agreement is not perfect between theory and experiment. For example, measured wavelength of a reflected pulse for a given pump-probe delay does not match with simulations. As we have pointed out in Ref. [28], the value of this wavelength depends on the pump pulse's space-time trajectory, which is set by the Raman-induced deceleration of the pump pulse. In general, it is difficult to model accurately the effect of Raman scattering on an ultrashort pump pulse, and the discrepancy can be attributed to that. It is worth noting that there is a secondary reflected pulse in Fig. 6(a) whose spectrum lies above that of the main reflected pulse. Its origin was traced to an unusual shape of input probe pulses. When we used the process of sum frequency generation for synchronization, we found that each probe pulse has a smaller subpulse trailing the main pulse by about 0.2 ps. This subpulse also reflects off the pump pulse and creates the secondary reflection peak. As the secondary reflection spectral peak is mostly a replica of the main peak, we will focus on it in the following sections.

4. IMPACT OF WIDER OR CHIRPED PUMP PULSES

In this section we focus on the impact of pump-pulse parameters on the temporal reflection of a probe pulse. More specifically, we consider two parameters, namely, the width and the chirp of pump pulses, and compare the results with the ideal case of an unchirped pump pulse launched with a width and energy such that it propagates as a fundamental soliton inside our PCF.

A. Effect of Wide Pump Pulses

We make the pump pulse wider by cutting down its spectral width by controlling the slit width inside the pulse shaper [see Fig. 3(b)]. The width of pump pulses was close to 162 fs when we reduced the spectral bandwidth to 11 nm. We used the frequency-resolved optical gating (FROG) technique to measure the width of input pump pulses. We also adjusted pulse's energy such that we obtain the same amount of Raman-induced red shift at the PCF's output. The probe pulses remain the same as before, and their spectrum is centered at 655 nm.

The experimental data for wider pump pulses is shown in the top row of Fig. 7 in the same format used for the narrower pump pulses in Fig. 6. The input pump spectrum in Fig. 7(b) is narrower (width 11 nm). The output spectrum has again two peaks, one at 800 nm, and the other at the red-shifted wavelength. The only difference is that more energy remains in the 800-nm region [37% of input energy compared to 12% in Fig. 6(b)]. This is because our wider pump pulse has a larger pulse energy and forms a higher-order soliton after entering the PCF. After a short distance, it breaks into multiple pulses of different widths through a fission-like process [29]. The shortest pulse evolves into a Raman soliton that shifts rapidly toward the red side.

The probe pulse spectra obtained when tuning the initial pump-probe delay are shown in Fig. 7(a). When we compare them to the probe spectra in Fig. 6, we notice similarities but also important differences. In the case of narrower soliton-like pulses

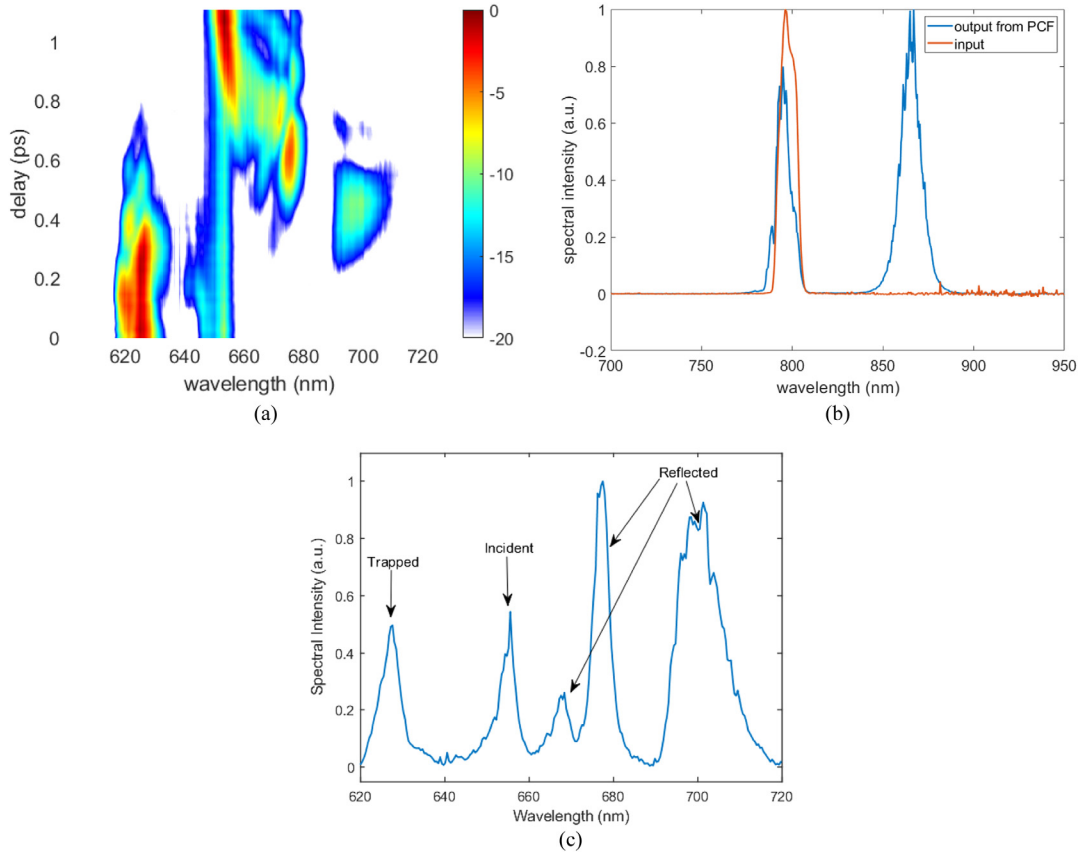

Fig. 7. Experimental results for wide pump pulses. (a) Spectra of probe pulses at the PCF output as the relative delay is varied. (b) Spectra of probe pulses at the input and output ends of the fiber. (c) Output spectrum obtained for a pump-probe delay of 0.5 ps. Three of the five peaks correspond to three reflected pulses.

shown in Fig. 6(a), a single reflected pulse is formed for any initial pump-probe delay. In contrast, multiple reflected pulses can form for wider pump pulses in a limited range of pump-probe delay. An example is shown in Fig. 7(c) for a specific delay of 0.5 ps. As seen there, temporal reflection results in three distinct spectral peaks that correspond to three reflected pulses.

To understand the physics better, we performed numerical simulations for wider pump pulses used in the experiment, and the results are shown in Fig. 8. For better accuracy, we used the shape of pump pulses deduced with the FROG technique for our simulations. Energy of the pump pulse was set to 18 pJ to ensure that the output Raman soliton matches with what we experimentally observed. This energy is equal to the energy of an $N = 2.5$ soliton with the same temporal FWHM (162 fs). The simulations in Fig. 8(a) show features similar to those observed experimentally in Fig. 7(a). In particular, multiple reflected pulses indeed form for specific pump-probe delays.

In both the experiments and numerical simulations, we observe a wide reflection peak around 700 nm for smaller pump-probe delays. As we increase this delay, in both cases we can identify a strong, narrow reflection peak near 680 nm for a delay of 0.6 ps or more. Also, transition from one peak to the other does not happen in a continuous fashion. This is different from the result shown in Fig. 6(a) for a fundamental soliton. The exact shape of the reflected spectrum also does not agree with the simulations. This is most probably related to the actual shapes of pump and probe pulses being different from those used in our simulations.

Figure 8(c) shows the temporal and spectral evolution of pump and probe pulses over the first 1-m length of the PCF. We only show the first 1 m of propagation here because the interaction of the pump pulse and probe pulse only takes place in this region. The input delay is chosen as 0.35 ps for this case. The pump pulse breaks into multiple pulses through soliton fission at a distance of about 15 cm. During the fission stage, the pump pulse has a complex intensity pattern, which produces a complex time dependence of the refractive index for the probe pulse. In the case shown in Fig. 8(c), the probe pulse interacts with different parts of the pump pulse at two distances, resulting in two reflected pulses with different spectral shifts. By comparing the results obtained for a fundamental soliton with those obtained for a higher-order soliton, we can conclude that the process of temporal reflection is sensitive to minute details of the evolution of the pump pulse. This is the reason why the output spectrum of probe pulses contains information about propagation dynamics of the pump pulse.

B. Effect of Chirped Pump Pulses

We next consider the case of chirped pump pulses. A simple way to chirp short pulses is to pass them though a dispersive delay line that broadens each pulse while also introducing some

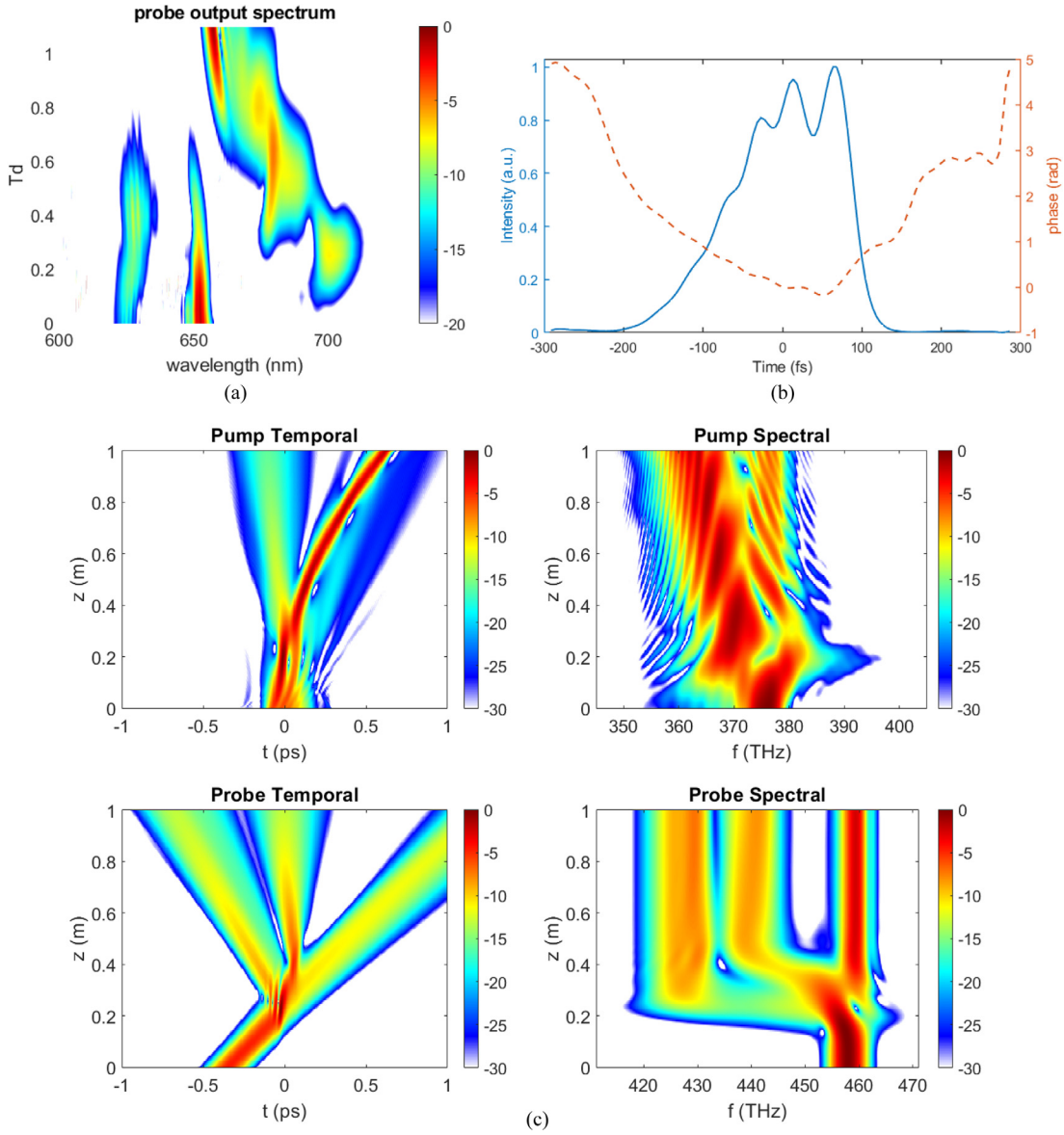

Fig. 8. Simulation results for wide pump pulses. (a) Spectra of probe pulses at the PCF output as the relative delay is varied. (b) Shape and chirp of the input pump pulse deduced with the FROG technique. (c) Evolution of the pump and probe pulses over the 1-m length of the PCF.

frequency chirp. We again use our pulse shaper for this purpose. The slit in the pulse shaper remains fully open, and no spectral filtering takes place. However, one of the prisms inside the pulse shaper is adjusted to introduce some positive chirp on the pump pulse. Before sending this pulse into the PCF, we characterize it with our FROG setup. The measured width is about 97 fs and corresponds to adding 1130 fs^2 of group-delay dispersion to a sech-shape pulse with 22-nm spectral width. The amount of pump pulse energy that couples into the PCF is also adjusted to ensure that the Raman soliton has the same 865-nm wavelength at the PCF's output as before.

The experimental results for chirped pump pulses are shown in Fig. 9. Figure 9(a) shows the output probe's output spectra measured while varying the relative pump-probe delay. Figure 9(b) compares the spectrum of the pump pulse at the input and output ends of the PCF. Similar to the case of wide pump pulses, chirping of the pump pulse increases energy remaining at the input wavelength of 800 nm but by a smaller amount.

The probe pulse spectra in Fig. 9(a) show a pattern different from the two earlier cases where an unchirped pump pulse forms a fundamental or a higher-order soliton. We expect these differences to result from a different evolution pattern occurring for chirped pump pulses. To confirm this expectation, we performed numerical simulations using the measured shape and phase of input pump pulses, and the results are shown in Fig. 10. Figure 10(a) shows the output probe spectra as a function of pump-probe delay. Figure 10(b) shows the shape and phase of input pump pulses obtained with our FROG setup. Figure 10(c) shows the temporal and spectral evolutions of the pump (top) and probe (bottom) pulses over the first 1 m of PCF.

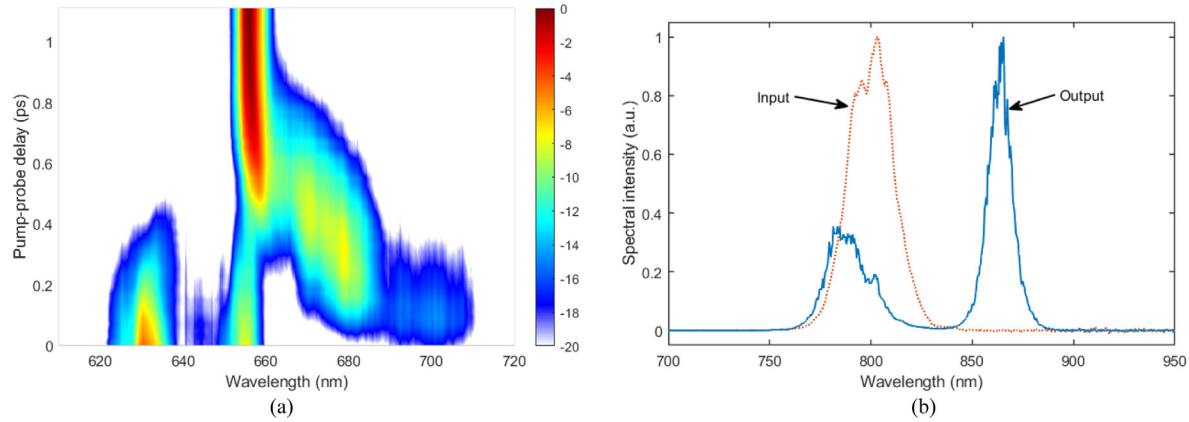

Fig. 9. Experimental results for chirped pump pulses. (a) Measured probe spectra at the PCF output as the relative pump-probe delay is varied from 0 to 1 ps. (b) Pump spectra at the input and output ends of the PCF.

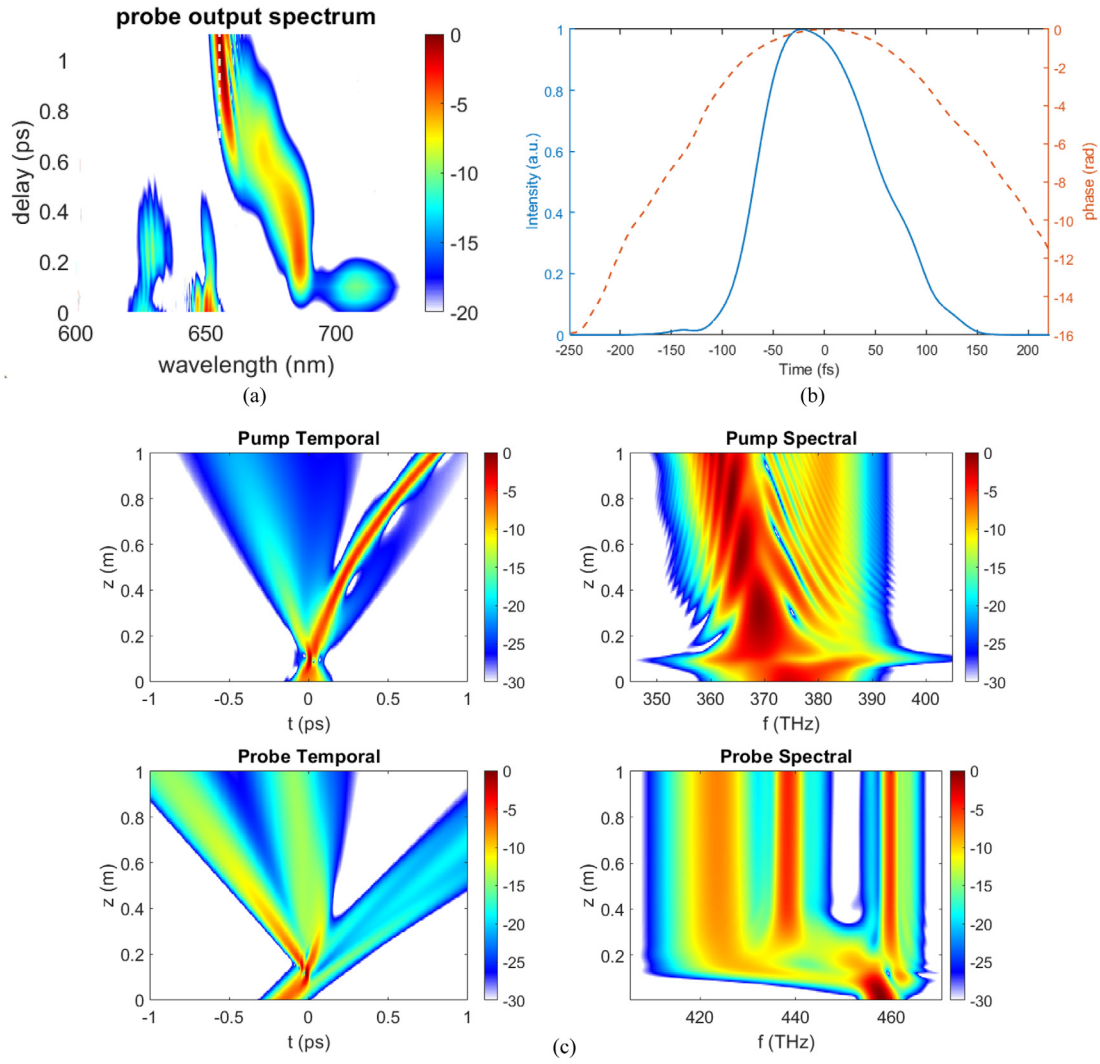

Fig. 10. Simulation results for chirped pump pulses. (a) Spectra of probe pulses at the PCF output as the relative delay is varied. (b) Shape and chirp of the input pump pulse deduced with the FROG technique. (c) Evolution of the pump and probe pulses over the 1-m length of the PCF.

A comparison of the simulated probe spectra with our experimental results in Fig. 9(a) shows a relatively good agreement. In particular, two reflected pulses are produced at different wavelengths when the pump-probe delay is <0.2 ps. In both simulations and experiments, the red shift of the main reflection peak decreases continuously as the delay is increased, and this

peak eventually merges with that of the incident probe pulse. We also observe a secondary reflection peak at a longer wavelength, but this peak exists only for smaller delays and disappears as delay increases.

Temporal and spectral evolutions of the pump and probe pulses are shown in Fig. 10(c) over the first 1 m of the PCF for a pump-probe delay of 0.15 ps. As seen there, the pump pulse is compressed considerably within the first 10 cm of PCF. At this point, the pulse splits into two parts. The majority of its energy forms a soliton that undergoes the Raman-induced red shift (red curve). The other part with remaining energy moves toward the left because it is blue-shifted and moves faster. This part does not form a soliton and disperses rapidly as it propagates. The effect that we observe here is related to the discussion in Ref. [35], where it was found that an intense pulse with chirp can split into two soliton-like pulses. We believe that it is this splitting of the pulse that is responsible for the two reflection peaks seen in Fig. 9(a) for small pump-probe delays. The wavelengths of the two reflected pulses shift by different amounts, resulting in the formation of two spectral peaks after a distance of 10 cm. We observed a similar behavior in our experiments when the pump-probe delay was small.

One more feature is noteworthy. Compared with the case of the pump pulse forming a higher-order soliton, the Raman soliton for chirped pump pulses is generated at a shorter distance. This implies that temporal reflection of the probe pulse should happen for smaller pump-probe delays. This is indeed what is observed when we compare the experimental results in Fig. 7(a) with those in Fig. 9(a). Comparing the observed behavior in the three cases of pump pulses (a fundamental soliton, a higher-order soliton, and a highly chirped pulse), we can conclude that temporal reflection is sensitive to different evolution dynamics of pump pulses occurring inside the PCF. This is the reason why measured probe spectra at the PCF's output can be used to deduce information such as deceleration of pump pulses initiated by the spectral shift induced by intrapulse Raman scattering.

5. CONCLUSIONS

In this paper, we have studied, through a series of experiments and simulations, how temporal reflection from an intense pump pulse is affected inside a PCF by the parameters of the pump pulse used to form a moving high-index boundary. We first studied the ideal case in which pump pulses form a short femtosecond soliton, whose spectrum red-shifts continuously inside the PCF because of intrapulse Raman scattering. In our experiments, most of the energy of 800-nm input pump pulses shifted to 865 nm over 3.8-m length of the fiber. Temporal reflection of a 655-nm probe pulse produced a single reflected pulse whose wavelength was shifted toward the red side by an amount that depends on the initial pump-probe delay.

We changed the width and chirp of our pump pulses in our experiments using a 4f pulse shaper, containing two prisms and a slit in the Fourier plane for spectral filtering. We found that temporal refection of probe pulses exhibited unexpected novel features when pump pulses were made wider through spectral filtering without much chirp. Similar but different features were observed when pulses were chirped through a dispersive delay line without any spectral filtering. In both cases, two or more reflected pulses were produced at different wavelengths in a specific range of initial pump-probe delays. Numerical simulations reveal that the origin of such novel features is related to a complex nonlinear evolution of pump pulses inside the PCF. Nonlinear phenomena such as the fission of higher-order solitons, intrapulse Raman scattering, and chirp-induced pulse compression can produce a temporal intensity pattern in pump pulses that is sensed by the probe pulse when it collides with a pump pulse at a distance that depends on initial pump-probe delay.

The observed novel effects can be interpreted as scattering of the probe wave from the pump's intensity pattern. When the pump pulse evolves as a fundamental soliton, its intensity forms a smooth high-index "mirror", and the probe's reflection produces a single red-shifted pulse at a shifted wavelength. However, when a more complex intensity pattern is formed for wider or chirped pump pulses, a probe can scatter from different parts of the pump pulse at different distances inside the PCF, resulting in multiple reflected pulses that are red-shifted by different amounts. This feature could, in principle, be used for studying the nonlinear evolution of a pump pulse with the PCF, without employing a destructive cut-back method. Temporal reflection is also useful for shifting the wavelength of a weak probe pulse when a suitable pump pulse is available.

Funding. National Science Foundation (ECCS-1933328); Department of Energy National Nuclear Security Administration (DE-NA0003856); University of Rochester; New York State Energy Research and Development Authority.

Acknowledgment. This report was prepared as an account of work sponsored by an agency of the U.S. Government. Neither the U.S. Government nor any agency thereof, nor any of their employees, makes any warranty, express or implied, or assumes any legal liability or responsibility for the accuracy, completeness, or usefulness of any information, apparatus, product, or process disclosed, or represents that its use would not infringe privately owned rights. Reference herein to any specific commercial product, process, or service by trade name, trademark, manufacturer, or otherwise does not necessarily constitute or imply its endorsement, recommendation, or favoring by the U.S. Government or any agency thereof. The views and opinions of authors expressed herein do not necessarily state or reflect those of the U.S. Government or any agency thereof.

Disclosures. The authors declare no conflicts of interest.

Data availability. Data underlying the results presented in this paper are not publicly available at this time but may be obtained from the authors upon reasonable request.

REFERENCES

1. E. Galiffi, R. Tirole, S. Yin, *et al.*, "Photonics of time-varying media," Adv. Photonics **4**, 014002 (2022).
2. M. A. Gaafar, T. Baba, M. Eich, *et al.*, "Front-induced transitions," Nat. Photonics **13**, 737–748 (2019).
3. C. Caloz and Z.-L. Deck-Léger, "Spacetime metamaterials–part I: general concepts," IEEE Trans. Antennas Propag. **68**, 1569–1582 (2019).
4. C. Caloz and Z.-L. Deck-Léger, "Spacetime metamaterials–part II: theory and applications," IEEE Trans. Antennas Propag. **68**, 1583–1598 (2019).
5. F. Miyamaru, C. Mizuo, T. Nakanishi, *et al.*, "Ultrafast frequency-shift dynamics at temporal boundary induced by structural-dispersion switching of waveguides," Phys. Rev. Lett. **127**, 053902 (2021).

6. H. Li and A. Alù, "Temporal switching to extend the bandwidth of thin absorbers," Optica **8**, 24–29 (2021).
7. R. Tirole, S. Vezzoli, E. Galiffi, *et al.*, "Double-slit time diffraction at optical frequencies," Nat. Phys. **19**, 999–1002 (2023).
8. F. R. Morgenthaler, "Velocity modulation of electromagnetic waves," IRE Trans. Microwave Theory Tech. **6**, 167–172 (1958).
9. Y. Xiao, D. N. Maywar, and G. P. Agrawal, "Reflection and transmission of electromagnetic waves at a temporal boundary," Opt. Lett. **39**, 574–577 (2014).
10. J. Mendonça and P. Shukla, "Time refraction and time reflection: two basic concepts," Phys. Scr. **65**, 160 (2002).
11. Y. Sharabi, A. Dikopoltsev, E. Lustig, *et al.*, "Spatiotemporal photonic crystals," Optica **9**, 585–592 (2022).
12. X. Wang, M. S. Mirmoosa, V. S. Asadchy, *et al.*, "Metasurface-based realization of photonic time crystals," Sci. Adv. **9**, eadg7541 (2023).
13. S. Saha, O. Segal, C. Fruhling, *et al.*, "Photonic time crystals: a materials perspective," Opt. Express **31**, 8267–8273 (2023).
14. V. Bacot, M. Labousse, A. Eddi, *et al.*, "Time reversal and holography with spacetime transformations," Nat. Phys. **12**, 972–977 (2016).
15. H. Moussa, G. Xu, S. Yin, *et al.*, "Observation of temporal reflection and broadband frequency translation at photonic time interfaces," Nat. Phys. **19**, 863–868 (2023).
16. Z. Dong, H. Li, T. Wan, *et al.*, "Quantum time reflection and refraction of ultracold atoms," Nat. Photonics **18**, 68–73 (2024).
17. B. W. Plansinis, W. R. Donaldson, and G. P. Agrawal, "What is the temporal analog of reflection and refraction of optical beams?" Phys. Rev. Lett. **115**, 183901 (2015).
18. J. Zhang, W. Donaldson, and G. P. Agrawal, "Temporal reflection of an optical pulse from a short soliton: impact of Raman scattering," J. Opt. Soc. Am. B **39**, 1950–1957 (2022).
19. W. Cai, H. Wu, Y. Liu, *et al.*, "Soliton and dispersive wave generation with third-order dispersion and temporal boundary," Opt. Express **32**, 7682–7696 (2024).
20. B. W. Plansinis, W. R. Donaldson, and G. P. Agrawal, "Temporal waveguides for optical pulses," J. Opt. Soc. Am. B **33**, 1112–1119 (2016).
21. B. W. Plansinis, W. R. Donaldson, and G. P. Agrawal, "Cross-phase-modulation-induced temporal reflection and waveguiding of optical pulses," J. Opt. Soc. Am. B **35**, 436–445 (2018).
22. J. Zhang, W. R. Donaldson, and G. P. Agrawal, "Temporal reflection and refraction of optical pulses inside a dispersive medium: an analytic approach," J. Opt. Soc. Am. B **38**, 997–1003 (2021).
23. J. Zhang, W. R. Donaldson, and G. P. Agrawal, "Impact of the boundary's sharpness on temporal reflection in dispersive media," Opt. Lett. **46**, 4053–4056 (2021).
24. T. G. Philbin, C. Kuklewicz, S. Robertson, *et al.*, "Fiber-optical analog of the event horizon," Science **319**, 1367–1370 (2008).
25. K. E. Webb, M. Erkintalo, Y. Xu, *et al.*, "Nonlinear optics of fibre event horizons," Nat. Commun. **5**, 4969 (2014).
26. L. Tartara, "Frequency shifting of femtosecond pulses by reflection at solitons," IEEE J. Quantum Electron. **48**, 1439–1442 (2012).
27. A. Demircan, S. Amiranashvili, and G. Steinmeyer, "Controlling light by light with an optical event horizon," Phys. Rev. Lett. **106**, 163901 (2011).
28. J. Zhang, W. R. Donaldson, and G. P. Agrawal, "Probing the decelerating trajectory of a Raman soliton using temporal reflection," Opt. Express **31**, 27621–27632 (2023).
29. G. P. Agrawal, *Nonlinear Fiber Optics*, 6th ed. (Academic, 2019).
30. P. Hlubina, M. Szpulak, D. Ciprian, *et al.*, "Measurement of the group dispersion of the fundamental mode of holey fiber by white-light spectral interferometry," Opt. Express **15**, 11073–11081 (2007).
31. T. Kardaś and C. Radzewicz, "Broadband near-infrared fibers dispersion measurement using white-light spectral interferometry," Opt. Commun. **282**, 4361–4365 (2009).
32. R. Fork, O. Martinez, and J. Gordon, "Negative dispersion using pairs of prisms," Opt. Lett. **9**, 150–152 (1984).
33. N. Nishizawa and T. Goto, "Pulse trapping by ultrashort soliton pulses in optical fibers across zero-dispersion wavelength," Opt. Lett. **27**, 152–154 (2002).
34. J. Zhang, W. Donaldson, and G. P. Agrawal, "Experimental observation of a Raman-induced temporal waveguide," Phys. Rev. A **107**, 063518 (2023).
35. D. Kaup, J. El-Reedy, and B. A. Malomed, "Effect of a chirp on soliton production," Phys. Rev. E **50**, 1635 (1994).